Photocatalytic Hydrogen Evolution from Substoichiometric Colloidal WO_{3-x} Nanowires

Taejong Paik,[†,⊥,∇] Matteo Cargnello,[†,#,∇] Thomas R. Gordon,[†] Sen Zhang,[†] Hongseok Yun,[†]
Jennifer D. Lee,[†] Ho Young Woo,[⊥] Soong Ju Oh,[‡,◆] Cherie R. Kagan,[†,‡,§] Paolo Fornasiero,[∥]
and Christopher B. Murray*[,†,‡]

[†]Department of Chemistry, University of Pennsylvania, Philadelphia, Pennsylvania 19104, United States

[‡]Department of Materials Science and Engineering, University of Pennsylvania, Philadelphia, Pennsylvania 19104, United States

[§]Department of Electrical and System Engineering, University of Pennsylvania, Philadelphia, Pennsylvania 19104, United States

[∥]Department of Chemical and Pharmaceutical Sciences, ICCOM-CNR, INSTM, University of Trieste, Trieste 34127, Italy

[⊥]School of Integrative Engineering, Chung-Ang University, Seoul, South Korea

[#]Department of Chemical Engineering, and SUNCAT Center for Interface Science and Catalysis, Stanford University, Stanford 94305, California United States

[◆]Department of Materials Science and Engineering, Korea University, Seoul, South Korea

Ⓢ *Supporting Information*

ABSTRACT: We report direct photocatalytic hydrogen evolution from substoichiometric highly reduced tungsten oxide (WO_x) nanowires (NWs) using sacrificial alcohol. WO_x NWs are synthesized via nonaqueous colloidal synthesis with a diameter of about 4 nm and an average length of about 250 nm. As-synthesized WO_x NWs exhibit a broad absorption across the visible to infrared regions attributed to the presence of oxygen vacancies. The optical band gap is increased in these WO_x NWs compared to stoichiometric bulk tungsten oxide (WO_3) powders as a result of the Burstein−Moss shift. As a consequence of this increase, we demonstrate direct photocatalytic hydrogen production from WO_x NWs through alcohol photoreforming. The stable H_2 evolution on platinized WO_x NWs is observed under conditions in which platinized bulk WO_3 and bulk $WO_{2.9}$ powders either do not show activity or show very low rates, suggesting that increased surface area and specific exposed facets are key for the improved performance of WO_x NWs. This work demonstrates that control of size and composition can lead to unexpected and beneficial changes in the photocatalytic properties of semiconductor materials.
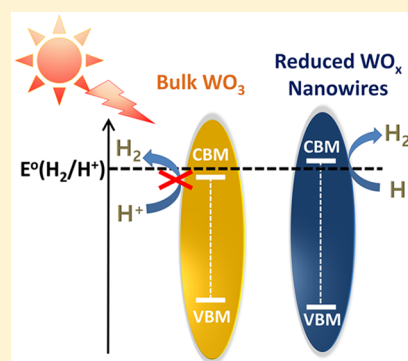
Solar energy conversion and storage are being heavily investigated in response to growing energy consumption and environmental concerns.[1] Solar-driven photocatalytic reactions catalyzed by semiconducting nanostructures are a promising class of processes to fulfill this demand. Among the various types of semiconducting solid-state materials, tungsten oxide is particularly interesting due to its unique optical properties and structural richness.[2,3] Tungsten oxide is a cheap, nontoxic, and earth-abundant material and has been widely used for many industrial applications such as electrochromic devices,[4−6] catalysts,[7,8] gas sensors,[9−11] and electronic devices.[12,13] Tungsten trioxide (WO_3) shows various stable crystal structures, and various oxygen-deficient, substoichiometric tungsten oxides, for example, $W_{20}O_{58}$, $W_{24}O_{68}$, and $W_{18}O_{49}$, are also stable in air.[2] Tungsten can possess variable oxidation states such as W(VI), W(V), and W(IV), which enables its utilization in charge storage and electrochromic device applications. Substoichiometric tungsten oxides are blue in color due to the emergence of defect states below the conduction band minimum, enabling lower-energy excitation from defect sites to the conduction bands[5] and strong light absorption in the near-infrared region, which is typically attributed to the excitation of free electrons in the conduction band derived from oxygen vacancies.[14]

Monoclinic WO_3 in bulk form has an indirect band gap of about 2.62 eV, which covers 12% of the energy range of the solar spectrum,[3] ideal for applications in solar energy utilization including photoelectrochemical cells,[15] CO_2 photoreduction,[16,17] and photocatalytic removal of pollutants.[7] In the past 3 decades, much work has focused on controlling the structure of tungsten oxide at the nanoscale in order to enhance its photocatalytic activity. For example, when the size
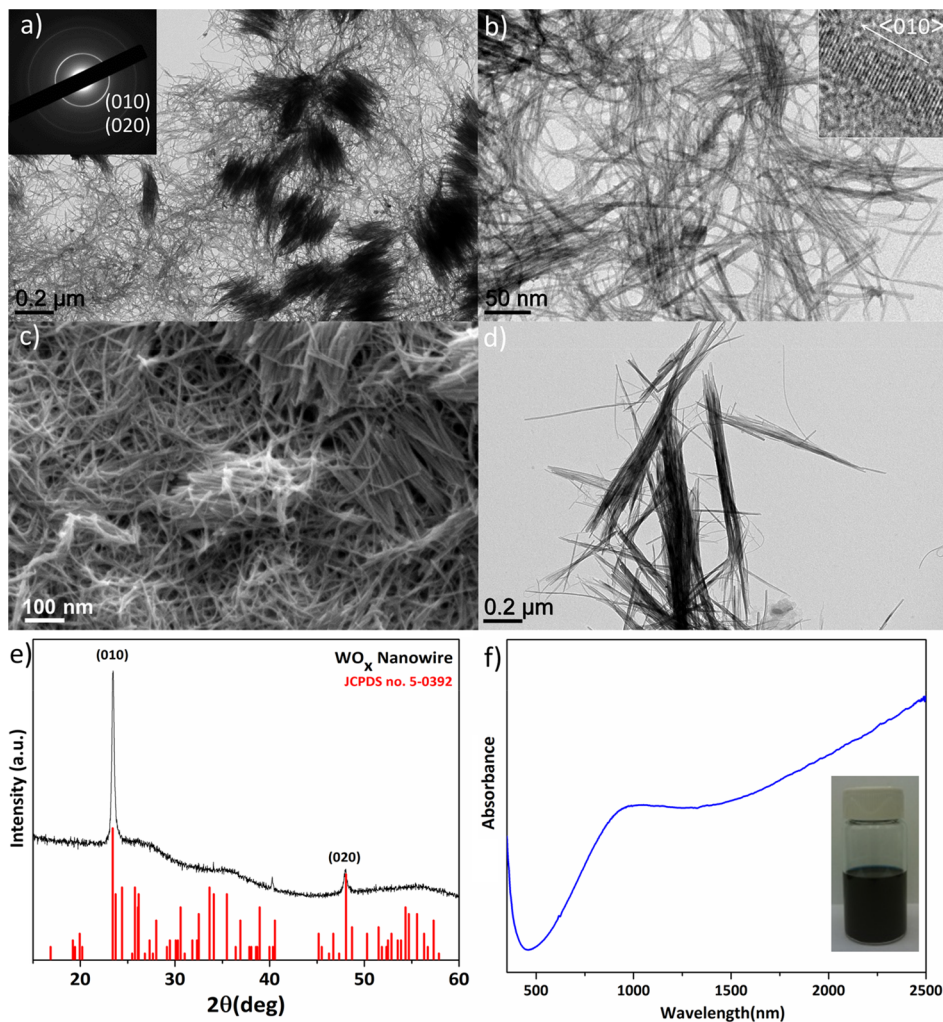
Figure 1. (a) Low-magnification TEM image of WO$_x$ NWs. The inset represents the wide-angle SAED pattern. (b) High-magnification TEM image. The inset shows the HRTEM image of a single WO$_x$ NW. (c) SEM image of WO$_x$ NWs. (d) TEM image of WO$_x$ NWs synthesized using trioctylamine solvent. (e) XRD pattern and (f) characteristic absorption spectra. The inset displays a photograph of WO$_x$ NWs dispersed in hexane.

of tungsten oxide nanocrystals (NCs) becomes smaller than the exciton Bohr radius, which is reported to be 3 nm, an increase in the band gap is observed.[18] Tight control of size,[19−21] shape,[22−24] stoichiometry,[25] and doping[26−28] of tungsten oxide allows precise control of the optical, electronic, and catalytic properties. Colloidal synthesis of WO$_x$ NCs and nanowires (NWs) has been reported by many in the literature,[21,29−31] yet the optical and catalytic properties have been limitedly investigated for a large number of shapes and structures. Therefore, it is important to investigate the structure−activity relationship in order to achieve the highest overall photocatalytic performance of tungsten oxide nanomaterials.

Here, we report the synthesis of oxygen-deficient WO$_x$ NWs via a high-temperature nonaqueous colloidal process. Highly uniform WO$_x$ NWs with a large aspect ratio, typically in the range between 50 and 250, and a very small diameter less than 5 nm are synthesized. These colloidal WO$_x$ NWs are dark navy blue in color due to their oxygen-deficiency. We examine the photoreforming reaction using reduced WO$_x$ NWs in the presence of alcohol. Photoreforming of oxygenated organic substances is a promising renewable process to produce H$_2$ over irradiated semiconductor surfaces and is widely studied

for many applications such as biomass-to-gas conversion[32] and photocatalytic degradation of organic pollutants.[33] In contrast to bulk samples, we observed stable hydrogen (H$_2$) evolution from our WO$_x$ NWs in photoreforming reactions using alcohols as electron donors. We attribute this behavior to the increased optical band gap in highly reduced substoichiometric WO$_x$ NWs from state-filling in one-dimensional thin NWs.

Colloidal tungsten oxide (WO$_x$) NCs are synthesized via high-temperature nonaqueous synthesis using tungsten hexa-chloride (WCl$_6$) as a metal precursor in the presence of 1-octadecanol and oleylamine. The reaction is conducted at 320 °C for 1 h in the absence of air and water. The color of the solution starts as greenish-blue and eventually turns dark navy blue when the temperature is approximately 300 °C, which likely is the starting point for the formation of WO$_x$ NWs in the reaction mixture. Figure 1a,b shows transmittance electron microscopy (TEM) and scanning electron microscopy (SEM) images of the as-produced WO$_x$ NWs. The diameter of each individual NW is approximately 4 nm on average, while their average length is about 250 nm. After drying on TEM grids, the NWs tend to assemble into large bundles, as displayed in Figure 1a,c, which may be attributed to van der Waals
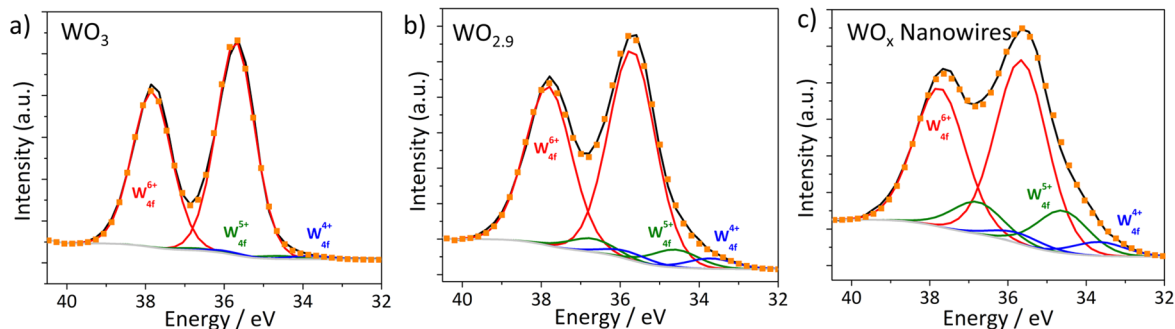
Figure 2. (a) XPS profiles of (a) bulk WO_3, (b) bulk $WO_{2.9}$, and (c) WO_x NWs.

interactions between the NWs with high aspect ratio and large surface-to-volume ratio.

The reaction occurs via the nonhydrolytic conversion of the metal halide into the oxide catalyzed by a primary alcohol.[34] In this reaction, the alcohol reacts with metal halides (M–X) to generate metal–hydroxyl (–W–OH) groups, followed by the condensation reaction to form metal oxide (M–O) bonds. This is further supported by observation that tungsten oxide NCs form only in the presence of an alcohol such as 1-octadecanol, oleyl alcohol, and 1,2-hexadecanediol. The addition of oleylamine in the reaction mixture alters the morphology and colloidal stability of NWs. In the absence of oleylamine, thicker WO_x nanorods are formed with a rough surface morphology, as displayed in Figure S1, and have poor colloidal stability. NWs produced in the presence of oleylamine have good colloidal stability, which indicates that oleylamine acts as a surfactant and stabilizing ligand. Longer NWs are obtained using trioctylamine as the solvent instead of oleylamine (Figure 1d). The length of the NWs can reach up to 1 μm without a noticeable change in the diameter. When trioctylamine is used, the color change of the reaction mixture is observed after 30 min at 320 °C, indicating slower growth kinetics as compared to oleylamine. The bulkiness of the tertiary amine is the likely origin of the slow growth, and the elongated structure is believed to derive from weaker stabilization of the wires during synthesis. The diffraction peaks from powder XRD analysis (Figure 1e) match the monoclinic WO_3 phase (JCPDS No. 5-0392). Relatively sharp peaks attributed to (010) and (020) crystallographic orientations indicate that NWs grow along the [010] direction, which is also corroborated by high-resolution transmission electron microscopy (HRTEM) images (Figure 1b inset).

As-synthesized NWs are dark navy in color due to their broad light absorption across the visible to the near-infrared (Figure 1f and inset). Coloration in relatively wide-band-gap n-type transition metal oxides has been previously reported, such as in titanium oxide (TiO_2)[35] and tungsten oxide (WO_x)[14] due to the formation of reduced species and oxygen vacancies. Other examples include indium-doped tin oxide (ITO),[36] indium-doped cadmium oxide (ICO),[37] and aluminum-doped zinc oxide (AZO),[38] which possess oxygen vacancies caused by doping of aliovalent metal impurities and indium oxide (In_2O_3)[39] and zinc oxide (ZnO)[40] NCs after photoreduction in which excited electrons populate the conduction band. Because of the reductive environment of the reaction conditions (320 °C) used during our synthesis, resulting from the presence of oleylamine and a 1-octadecanol mixture, which are known as mild chemical reductants,[41,42] a further reduction of the tungsten precursor is believed to occur than

would otherwise be observed under typical conditions. Nonstoichiometric phases of tungsten oxides result in the generation of oxygen vacancies or interstitial defects, which provide additional electrons to the conduction band. This enables Drude-like absorption from free-electron oscillations in the NCs.[14] The blue coloration of reduced species is also observed in commercially available reduced $WO_{2.9}$ powder, while stoichiometric tungsten oxide (WO_3) is greenish-yellow in color. X-ray photoelectron spectroscopy (XPS) studies are conducted to examine the compositions and valence states of tungsten in bulk samples and as-synthesized NWs. Figure 2 shows a high-resolution W_{4f} XPS spectrum and deconvolution results of the $W_{4f7/2}$ peaks for bulk WO_3, bulk $WO_{2.9}$, and WO_x NWs synthesized in this work. The relative ratios of tungsten components with different oxidation states are tabulated in Table 1. Bulk WO_3 powders contain mostly W(VI) oxidation

Table 1. Relative Ratio of Tungsten Components with Different Oxidation States Calculated from the XPS W_{4f} Spectra

	W^{6+} (%)	W^{5+} (%)	W^{4+} (%)
bulk WO_3	97.0	1.40	1.60
$WO_{2.9}$	88.12	7.51	4.37
WO_x NWs	77.65	17.93	4.42

state, while W(VI), W(V), and W(IV) states all coexist in the $WO_{2.9}$ bulk powders. The relative amount of W(V) and W(IV) compositions is even higher in the as-synthesized WO_x NWs, indicating that substoichiometric WO_x NWs contain more reduced W species and that a large quantity of the oxygen vacancies is introduced.

The increase of dopant concentration or oxygen defects in n-type metal oxide semiconductors results in an increase of the optical band gap, which is referred to as a Burstein–Moss shift.[37,43] The absorption edge of a degenerate semiconductor is increased to more negative potentials as a result of filling states. To investigate the optical band gap of nonstoichiometric tungsten oxide samples, we measure the diffuse reflectance spectra of bulk WO_3, bulk $WO_{2.9}$, and WO_x NWs. Figure 3a shows Kubelka–Munk plots of bulk WO_3, bulk $WO_{2.9}$, and WO_x NWs. The optical band gap of stoichiometric WO_3 is 2.67 eV, which is in agreement with the reported bulk value for monoclinic WO_3.[2] A large shift of the band gap to 3.05 eV is observed in the reduced $WO_{2.9}$ bulk powder, indicative of the effect of oxygen vacancies. A further increase in the band gap of as-synthesized WO_x NWs to 3.17 eV is found, which is attributed to the increase of oxygen vacancies resulting from reduced tungsten states in substoichiometric WO_x NWs. The
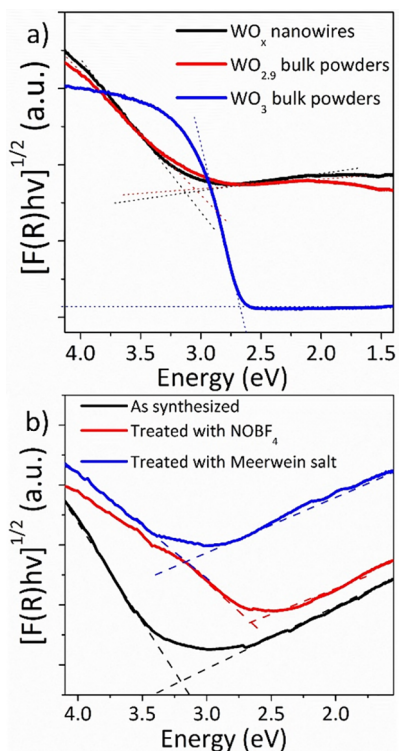
3

Figure 3. (a) Diffuse reflectance spectra of bulk WO_3, bulk $WO_{2.9}$, and WO_x NWs and (b) WO_x NWs before and after surface modification with $NOBF_4$ and Meerwein's salts.

further shift of the optical band gap of WO_x NWs as compared to commercial $WO_{2.9}$ is corroborated by the increased concentration of reduced tungsten species found by XPS (see above).

To investigate the effect of the oxidation state of tungsten in WO_x NWs on the optical band gap, we conducted chemical treatments with nitrosonium tetrafluoroborate ($NOBF_4$) and triethyloxonium tetrafluoroborate ((C_2H_5)$_3OBF_4$ or Meerwein's salt). Both chemicals replace the long organic ligands and leave identical species (BF_4^-) on the surface of NWs; however, $NOBF_4$ is known as a strong oxidizing agent[44] while Meerwein's salts are known to be milder.[45] XPS results indicate an increase of the relative amount of W(VI) and W(V) compositions in WO_x NWs after $NOBF_4$ treatment(Figure S2, Table S1). In agreement with their strength, a red shift of the band gap from 3.17 to 2.69 eV after ligand exchange of the WO_x NWs is observed using $NOBF_4$, with their color turning to greenish-blue. On the contrary, no shift of the band gap is observed after ligand exchange using Meerwein's salt (Figure 3b), and both the morphology of NWs and their color are preserved.

Photocatalytic hydrogen production by photoreforming is carried out by dispersing the nanopowders in water/alcohol mixtures and irradiating with UV/vis light.[46] For the systematic studies of colloidal NC suspensions, we conduct surface ligand exchange with Meerwein's salts in order to improve the dispersibility of the as-synthesized WO_x NWs in polar solvents. Platinum (Pt) is photodeposited as a co-catalyst with 1 wt % loading on the WO_x NWs in order to kinetically favor the formation of H_2 molecules and to act as an electron collector. Experiments in the absence of Pt or in the dark did not give any appreciable H_2 evolution. TEM images show that the average particle size of Pt deposited on WO_x NWs is <3 nm in

diameter (Figure S3) and is very similar between different samples. For the control experiments, we conduct the photocatalytic reaction using commercial stoichiometric WO_3 powders (yellow) and reduced $WO_{2.9}$ powders (blue) also added with Pt. The reduced, commercial $WO_{2.9}$ powder has comparable stoichiometry to the WO_x NWs but lower exposed surface area and does not preferentially expose any particular facet. Figure 4a shows the rate of H_2 production of Pt/WO_x
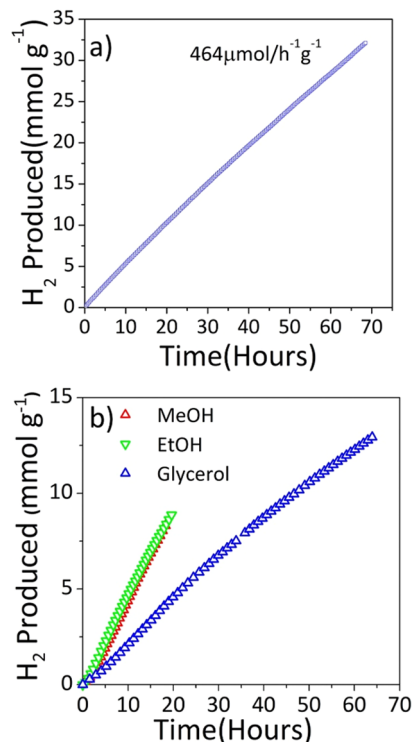

Figure 4. (a) Hydrogen evolution over time from 1 wt % Pt-loaded WO_x NWs under UV/vis light illumination (150 W Hg−Xe arc lamp) in 1:1 vol. mixtures of MeOH/H_2O. (b) Hydrogen evolution using a Pt/WO_x NW catalyst in different types of sacrificial agents (methanol, ethanol, and glycerol).

NWs in water/methanol solution (50/50 vol %) under UV/vis illumination. The color of BF_4-treated and platinized WO_x NWs further deepens under steady-state illumination, which could be due to accumulation of photoreduced carriers in the conduction band inducing enhanced absorption in visible to near-IR range[39] or to hydrogen intercalation in the WO_x structure. Under identical reaction conditions, stoichiometric and platinized WO_3 exhibits no activity for H_2 evolution because the position of its conduction band is more positive than the H_2 reduction potential.[47] We also tested the catalytic activity of platinized bulk $WO_{2.9}$ powder and observed no hydrogen evolution under irradiation. Interestingly, however, it was found that when using a much larger mass of $WO_{2.9}$ photocatalyst from a particular vendor (Alfa Aesar) to compensate for the lower surface area of this sample, a small but non-negligible amount of H_2 was produced (<20 μmol h^{-1} g^{-1}). Despite this, comparably high and stable H_2 evolution is observed from the ligand-exchanged WO_x NWs under UV/vis irradiation. The H_2 evolution of Pt/WO_x catalysts is observed in the presence of different types of sacrificial agents. Figure 4b exhibits fairly constant H_2 evolution from Pt/WO_x nano-catalysts in methanol and ethanol (up to 50 vol % in H_2O) and

glycerol (1 M in H_2O). The H_2 evolution of Pt/WO$_x$ NWs in the presence of methanol and ethanol occurs at almost identical rates, suggesting that the first dehydrogenation involving the primary OH group is the fastest step, while photoreforming from glycerol occurs at approximately half of the H_2 evolution rate, which may be attributed to the bulkiness of this sacrificial reagent in the photoreforming reaction and the fact that glycerol has secondary hydroxyl groups.[48] Slow CO_2 evolution is observed from all samples, demonstrating that the dehydrogenation process is likely prevalent over complete photoreforming under these conditions.[49] When a bandpass filter was used to remove the UV radiation, no hydrogen evolution was observed from the WO$_x$ NW sample, further suggesting that the change in the position of the conduction band and the increase of its band gap are the reasons for the observed hydrogen production under UV illumination.

In order to probe the electronic structures of the conduction band minimum and valence band maximum, we examine our materials using ultraviolet photoelectron spectroscopy (UPS). Figure 5a represents the secondary electron cutoffs and the valence band spectra of WO$_3$, WO$_{2.9}$, Meerwein's salt-treated WO$_x$−BF$_4$ NWs, and NOBF$_4$-treated WO$_x$−BF$_4$ NWs. The ionization energies of each sample are calculated by summation of the work function and the valence band maximum relative to the Fermi energy level. The position of the conduction band minimum is estimated using the optical band gaps of samples obtained from diffuse reflectance spectra (DRS) measurements. Figure 5b represents the energy diagrams, showing the HOMO−LUMO energy levels of WO$_3$, WO$_{2.9}$, and WO$_x$ NWs with respect to the standard hydrogen reduction potentials. As reported in many references, the conduction band minimum of the WO$_3$ powders is lower than the reduction potential of the H^+/H_2 couple, which explains why direct photocatalytic hydrogen evolution is not possible using stoichiometric WO$_3$. The position of the valence band maximum of reduced WO$_{2.9}$ powder is nearly identical to that of WO$_3$ powder; however, the oxygen deficiency shifts the conduction band minimum to a more negative potential than stoichiometric WO$_3$. In the case of reduced WO$_x$ NWs, an increase in the ionization potential is observed due to lowering of the position of the valence band maximum, which results in a widening of its band gap NWs. As a result, the conduction band edge of reduced WO$_x$ NWs (and commercial WO$_{2.9}$) is negative enough to achieve proton reduction and generate H_2. In contrast, oxidized WO$_x$ NWs show an increase in work function, which may be attributed to the adsorption of oxygen-rich impurities on the surface during NOBF$_4$ treatments.[50,51] Therefore, the conduction band maximum of oxidized WO$_x$ NWs becomes more positive than the standard hydrogen reduction potential, which suggests that substantial oxygen deficiency is necessary to induce the direct photocatalytic hydrogen evolution of tungsten oxide. In this sense, the fact that the commercial WO$_{2.9}$ sample also showed H_2 production, albeit at very modest rates, is a further indication that the reduction of tungsten oxide and the subsequent shift of the CB position are at the origin of the H_2 evolution activity of this sample. The much higher H_2 production rate in the WO$_x$ NW material is probably due to the much larger exposed surface area and to the preferential exposure of particular facets on the NW sides.

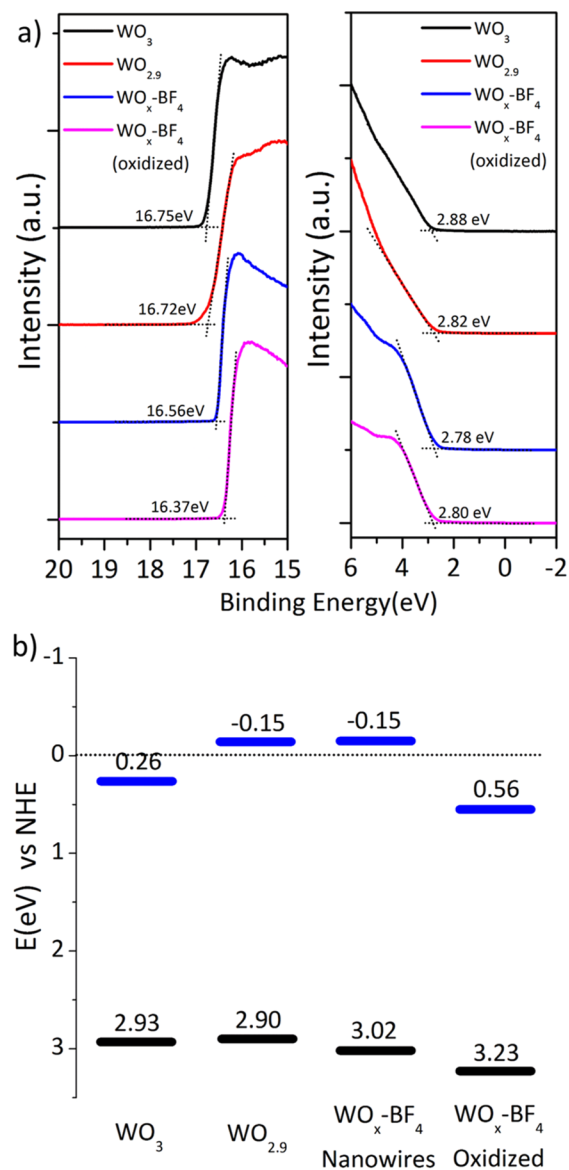In summary, we demonstrate photocatalytic hydrogen generation from blue WO$_x$ NWs. WO$_x$ NWs are synthesized

Figure 5. (a) UPS spectra of WO$_3$, WO$_{2.9}$, WO$_x$−BF$_4$ NWs, and oxidized WO$_x$−BF$_4$ NWs. The UPS spectra of the secondary electron edge and the valence bands are measured with He1(21.2 eV) radiation. (b) Energy levels are calculated by UPS results and the optical band gap.

via a high-temperature nonhydrolytic condensation reaction in the presence of WCl$_6$ and 1-octadecanol with high size and shape uniformity. Blue coloration from colloidal WO$_x$ NWs is observed due to oxygen deficiency in the material resulting from the synthesis performed in a highly reductive environment. Broadening of the optical band gap is observed in highly reduced substoichiometric WO$_x$ NWs, which is attributed to the self-doping of W^{5+} and W^{4+} resulting in the oxygen vacancies. We demonstrate stable photocatalytic H_2 evolution using alcohols as sacrificial agents, which indicates that the conduction band in reduced WO$_x$ NWs becomes more negative than the standard hydrogen reduction potential, which is not achievable in bulk WO$_3$. The novel synthesis of self-doped WO$_x$ NWs provides a route to design efficient catalytic building blocks for the development of sustainable solar-light conversion systems.

■ AUTHOR INFORMATION

Corresponding Author

*E-mail: cbmurray@sas.upenn.edu.

ORCID ⓞ

Taejong Paik: 0000-0003-0111-8513

Matteo Cargnello: 0000-0002-7344-9031

Sen Zhang: 0000-0002-1716-3741

Hongseok Yun: 0000-0003-0497-6185

Jennifer D. Lee: 0000-0003-2644-3507

Soong Ju Oh: 0000-0003-1434-8844

Cherie R. Kagan: 0000-0001-6540-2009

Paolo Fornasiero: 0000-0003-1082-9157

Author Contributions

[∇]T.P and M. C contributed equally to this work. The manuscript was written through contributions of all authors. All authors have given approval to the final version of the manuscript.

Notes

The authors declare no competing financial interest.

■ REFERENCES

(1) Lewis, N. S.; Nocera, D. G. Powering the Planet: Chemical Challenges in Solar Energy Utilization. *Proc. Natl. Acad. Sci. U. S. A.* **2006**, *103*, 15729−15735.

(2) Zheng, H.; Ou, J. Z.; Strano, M. S.; Kaner, R. B.; Mitchell, A.; Kalantar-zadeh, K. Nanostructured Tungsten Oxide − Properties, Synthesis, and Applications. *Adv. Funct. Mater.* **2011**, *21*, 2175.

(3) Huang, Z.-F.; Song, J.; Pan, L.; Zhang, X.; Wang, L.; Zou, J.-J. Tungsten Oxides for Photocatalysis, Electrochemistry, and Phototherapy. *Adv. Mater.* **2015**, *27*, 5309−5327.

(4) Granqvist, C. G. Electrochromic Tungsten Oxide Films: Review of Progress 1993−1998. *Sol. Energy Mater. Sol. Cells* **2000**, *60*, 201−262.

(5) Deb, S. K. Opportunities and Challenges in Science and Technology of WO_3 for Electrochromic and Related Applications. *Sol. Energy Mater. Sol. Cells* **2008**, *92*, 245−258.

(6) Liu, J.-W.; Zheng, J.; Wang, J.-L.; Xu, J.; Li, H.-H.; Yu, S.-H. Ultrathin $W_{18}O_{49}$ Nanowire Assemblies for Electrochromic Devices. *Nano Lett.* **2013**, *13*, 3589−3593.

(7) Abe, R.; Takami, H.; Murakami, N.; Ohtani, B. Pristine Simple Oxides as Visible Light Driven Photocatalysts: Highly Efficient Decomposition of Organic Compounds over Platinum-Loaded Tungsten Oxide. *J. Am. Chem. Soc.* **2008**, *130*, 7780−7781.

(8) Hodes, G.; Cahen, D.; Manassen, J. Tungsten Trioxide as a Photoanode for a Photoelectrochemical Cell (PEC). *Nature* **1976**, *260*, 312−313.

(9) Polleux, J.; Gurlo, A.; Barsan, N.; Weimar, U.; Antonietti, M.; Niederberger, M. Template-Free Synthesis and Assembly of Single-Crystalline Tungsten Oxide Nanowires and their Gas-Sensing Properties. *Angew. Chem., Int. Ed.* **2006**, *45*, 261−265.

(10) Xiang, Q.; Meng, G. F.; Zhao, H. B.; Zhang, Y.; Li, H.; Ma, W. J.; Xu, J. Q. Au Nanoparticle Modified WO_3 Nanorods with Their Enhanced Properties for Photocatalysis and Gas Sensing. *J. Phys. Chem. C* **2010**, *114*, 2049−2055.

(11) Solis, J. L.; Saukko, S.; Kish, L.; Granqvist, C. G.; Lantto, V. Semiconductor Gas Sensors Based on Nanostructured Tungsten Oxide. *Thin Solid Films* **2001**, *391*, 255−260.

(12) Tao, C.; Ruan, S.; Xie, G.; Kong, X.; Shen, L.; Meng, F.; Liu, C.; Zhang, X.; Dong, W.; Chen, W. Role of Tungsten Oxide in Inverted Polymer Solar Cells. *Appl. Phys. Lett.* **2009**, *94*, 043311−043311.

(13) Meyer, J.; Winkler, T.; Hamwi, S.; Schmale, S.; Johannes, H.-H.; Weimann, T.; Hinze, P.; Kowalsky, W.; Riedl, T. Transparent Inverted Organic Light-Emitting Diodes with a Tungsten Oxide Buffer Layer. *Adv. Mater.* **2008**, *20*, 3839−3843.

(14) Manthiram, K.; Alivisatos, A. P. Tunable Localized Surface Plasmon Resonances in Tungsten Oxide Nanocrystals. *J. Am. Chem. Soc.* **2012**, *134*, 3995−3998.

(15) Hardee, K. L.; Bard, A. J. Semiconductor Electrodes X. Photoelectrochemical Behavior of Several Polycrystalline Metal Oxide Electrodes in Aqueous Solutions. *J. Electrochem. Soc.* **1977**, *124*, 215−224.

(16) Xi, G.; et al. Ultrathin $W_{18}O_{49}$ Nanowires with Diameters below 1 nm: Synthesis, Near-Infrared Absorption, Photoluminescence, and Photochemical Reduction of Carbon Dioxide. *Angew. Chem., Int. Ed.* **2012**, *51*, 2395−2399.

(17) Chen, X.; Zhou, Y.; Liu, Q.; Li, Z.; Liu, J.; Zou, Z. Ultrathin, Single-Crystal WO_3 Nanosheets by Two-Dimensional Oriented Attachment toward Enhanced Photocatalystic Reduction of CO_2 into Hydrocarbon Fuels under Visible Light. *ACS Appl. Mater. Interfaces* **2012**, *4*, 3372−3377.

(18) Gullapalli, S. K.; Vemuri, R. S.; Ramana, C. V. Structural Transformation Induced Changes in the Optical Properties of Nanocrystalline Tungsten Oxide Thin Films. *Appl. Phys. Lett.* **2010**, *96*, 171903.

(19) Tanaka, D.; Oaki, Y.; Imai, H. Enhanced Photocatalytic Activity of Quantum-Confined Tungsten Trioxide Nanoparticles in Mesoporous Silica. *Chem. Commun.* **2010**, *46*, 5286−5288.

(20) Liu, J.; Margeat, O.; Dachraoui, W.; Liu, X.; Fahlman, M.; Ackermann, J. Gram-Scale Synthesis of Ultrathin Tungsten Oxide Nanowires and their Aspect Ratio-Dependent Photocatalytic Activity. *Adv. Funct. Mater.* **2014**, *24*, 6029−6037.

(21) Moshofsky, B.; Mokari, T. Length and Diameter Control of Ultrathin Nanowires of Substoichiometric Tungsten Oxide with Insights into the Growth Mechanism. *Chem. Mater.* **2013**, *25*, 1384−1391.

(22) Waller, M. R.; Townsend, T. K.; Zhao, J.; Sabio, E. M.; Chamousis, R. L.; Browning, N. D.; Osterloh, F. E. Single-Crystal Tungsten Oxide Nanosheets: Photochemical Water Oxidation in the Quantum Confinement Regime. *Chem. Mater.* **2012**, *24*, 698−704.

(23) Zhao, Z.-G.; Liu, Z.-F.; Miyauchi, M. Nature-Inspired Construction, Characterization, and Photocatalytic Properties of Single-Crystalline Tungsten Oxide Octahedra. *Chem. Commun.* **2010**, *46*, 3321−3323.

(24) Xie, Y. P.; Liu, G.; Yin, L.; Cheng, H.-M. Crystal Facet-Dependent Photocatalytic Oxidation and Reduction Reactivity of Monoclinic WO_3 for Solar Energy Conversion. *J. Mater. Chem.* **2012**, *22*, 6746−6751.

(25) Zhao, J.; Olide, E.; Osterloh, F. E. Enhancing Majority Carrier Transport in WO$_3$ Water Oxidation Photoanode via Electrochemical Doping. *J. Electrochem. Soc.* **2015**, *162*, H65−H71.

(26) Cole, B.; Marsen, B.; Miller, E.; Yan, Y.; To, B.; Jones, K.; Al-Jassim, M. Evaluation of Nitrogen Doping of Tungsten Oxide for Photoelectrochemical Water Splitting. *J. Phys. Chem. C* **2008**, *112*, 5213−5220.

(27) Wang, F.; Di Valentin, C.; Pacchioni, G. Doping of WO$_3$ for Photocatalytic Water Splitting: Hints from Density Functional Theory. *J. Phys. Chem. C* **2012**, *116*, 8901−8909.

(28) Mi, Q.; Ping, Y.; Li, Y.; Cao, B.; Brunschwig, B. S.; Khalifah, P. G.; Galli, G. A.; Gray, H. B.; Lewis, N. S. Thermally Stable N$_2$-Intercalated WO$_3$ Photoanodes for Water Oxidation. *J. Am. Chem. Soc.* **2012**, *134*, 18318−18324.

(29) Lee, K.; Seo, W. S.; Park, J. T. Synthesis and Optical Properties of Colloidal Tungsten Oxide Nanorods. *J. Am. Chem. Soc.* **2003**, *125*, 3408−3409.

(30) Niederberger, M.; Bartl, M. H.; Stucky, G. D. Benzyl Alcohol and Transition Metal Chlorides as a Versatile Reaction System for the Nonaqueous and Low-Temperature Synthesis of Crystalline Nano-Objects with Controlled Dimensionality. *J. Am. Chem. Soc.* **2002**, *124*, 13642−13643.

(31) Polleux, J.; Pinna, N.; Antonietti, M.; Niederberger, M. Growth and Assembly of Crystalline Tungsten Oxide Nanostructures Assisted by Bioligation. *J. Am. Chem. Soc.* **2005**, *127*, 15595−15601.

(32) Kawai, T.; Sakata, T. Photocatalytic Hydrogen Production from Liquid Methanol and Water. *J. Chem. Soc., Chem. Commun.* **1980**, 694−695.

(33) Patsoura, A.; Kondarides, D. I.; Verykios, X. E. Photocatalytic Degradation of Organic Pollutants with Simultaneous Production of Hydrogen. *Catal. Today* **2007**, *124*, 94−102.

(34) Niederberger, M. Nonaqueous Sol−Gel Routes to Metal Oxide Nanoparticles. *Acc. Chem. Res.* **2007**, *40*, 793−800.

(35) Gordon, T. R.; Cargnello, M.; Paik, T.; Mangolini, F.; Weber, R. T.; Fornasiero, P.; Murray, C. B. Nonaqueous Synthesis of TiO$_2$ Nanocrystals Using TiF$_4$ to Engineer Morphology, Oxygen Vacancy Concentration, and Photocatalytic Activity. *J. Am. Chem. Soc.* **2012**, *134*, 6751−6761.

(36) Kanehara, M.; Koike, H.; Yoshinaga, T.; Teranishi, T. Indium Tin Oxide Nanoparticles with Compositionally Tunable Surface Plasmon Resonance Frequencies in the Near-IR Region. *J. Am. Chem. Soc.* **2009**, *131*, 17736−17736.

(37) Gordon, T. R.; Paik, T.; Klein, D. R.; Naik, G. V.; Caglayan, H.; Boltasseva, A.; Murray, C. B. Shape-Dependent Plasmonic Response and Directed Self-Assembly in a New Semiconductor Building Block, Indium-Doped Cadmium Oxide (ICO). *Nano Lett.* **2013**, *13*, 2857−2863.

(38) Buonsanti, R.; Llordes, A.; Aloni, S.; Helms, B. A.; Milliron, D. J. Tunable Infrared Absorption and Visible Transparency of Colloidal Aluminum-Doped Zinc Oxide Nanocrystals. *Nano Lett.* **2011**, *11*, 4706−4710.

(39) Schimpf, A. M.; Lounis, S. D.; Runnerstrom, E. L.; Milliron, D. J.; Gamelin, D. R. Redox Chemistries and Plasmon Energies of Photodoped In$_2$O$_3$ and Sn-Doped In$_2$O$_3$ (ITO) Nanocrystals. *J. Am. Chem. Soc.* **2015**, *137*, 518−524.

(40) Schimpf, A. M.; Gunthardt, C. E.; Rinehart, J. D.; Mayer, J. M.; Gamelin, D. R. Controlling Carrier Densities in Photochemically Reduced Colloidal ZnO Nanocrystals: Size Dependence and Role of the Hole Quencher. *J. Am. Chem. Soc.* **2013**, *135*, 16569−16577.

(41) Mourdikoudis, S.; Liz-Marzan, L. M. Oleylamine in Nanoparticle Synthesis. *Chem. Mater.* **2013**, *25*, 1465−1476.

(42) Sun, S.; Zeng, H. Size-Controlled Synthesis of Magnetite Nanoparticles. *J. Am. Chem. Soc.* **2002**, *124*, 8204−8205.

(43) Wang, A.; Babcock, J. R.; Edleman, N. L.; Metz, A. W.; Lane, M. A.; Asahi, R.; Dravid, V. P.; Kannewurf, C. R.; Freeman, A. J.; Marks, T. J. Indium-Cadmium-Oxide Films Having Exceptional Electrical Conductivity And Optical Transparency: Clues for Optimizing Transparent Conductors. *Proc. Natl. Acad. Sci. U. S. A.* **2001**, *98*, 7113−7116.

(44) Dong, A.; Ye, X.; Chen, J.; Kang, Y.; Gordon, T.; Kikkawa, J. M.; Murray, C. B. A Generalized Ligand-Exchange Strategy Enabling Sequential Surface Functionalization of Colloidal Nanocrystals. *J. Am. Chem. Soc.* **2011**, *133*, 998−1006.

(45) Rosen, E. L.; Buonsanti, R.; Llordes, A.; Sawvel, A. M.; Milliron, D. J.; Helms, B. A. Exceptionally Mild Reactive Stripping of Native Ligands from Nanocrystal Surfaces by Using Meerwein's Salt. *Angew. Chem., Int. Ed.* **2012**, *51*, 684−689.

(46) Kondarides, D. I.; Daskalaki, V. M.; Patsoura, A.; Verykios, X. E. Hydrogen Production by Photo-Induced Reforming of Biomass Components and Derivatives at Ambient Conditions. *Catal. Lett.* **2008**, *122*, 26−32.

(47) Jana, N. R.; Gearheart, L.; Murphy, C. J. Wet Chemical Synthesis of High Aspect Ratio Cylindrical Gold Nanorods. *J. Phys. Chem. B* **2001**, *105*, 4065−4067.

(48) Cargnello, M.; Gasparotto, A.; Gombac, V.; Montini, T.; Barreca, D.; Fornasiero, P. Photocatalytic H$_2$ and Added-Value By-Products − The Role of Metal Oxide Systems in Their Synthesis from Oxygenates. *Eur. J. Inorg. Chem.* **2011**, *2011*, 4309−4323.

(49) Montini, T.; Gombac, V.; Sordelli, L.; Delgado, J. J.; Chen, X.; Adami, G.; Fornasiero, P. Nanostructured Cu/TiO$_2$ Photocatalysts for H$_2$ Production from Ethanol and Glycerol Aqueous Solutions. *ChemCatChem* **2011**, *3*, 574−577.

(50) Irfan, Irfan; Turinske, A. J.; Bao, Z.; Gao, Y. Work Function Recovery of Air Exposed Molybdenum Oxide Thin Films. *Appl. Phys. Lett.* **2012**, *101*, 093305.

(51) Höchst, H.; Bringans, R. D. Electronic Structure of Evaporated and Annealed Tungsten Oxide Films Studied with UPS. *Appl. Surf. Sci.* **1982**, *11−12*, 768−773.